

tmp title: MUSC source

Damien Pageot^{*†}, Donatiennne Leparoux*, Mathieu Le Feuvre*, Olivier
Durand* and Yann Capdeville[‡]

^{*}*LUNAM-IFSTTAR*,

[†]*OSUNA*

^{*}*LPGN*,

(June 3, 2015)

GEO-Example

Running head: *Geophysics example*

ABSTRACT

INTRODUCTION

Since decades, geophysicists develop numerical inversion and imaging methods for seismic measurements (receiver function analysis (Ammon, 1991), ray-based methods (Jones, 2013), finite-frequency tomography (Montelli et al., 2004), inversion-based methods (Virieux and Operto, 2009)) to determine the structures and the physical properties of the Earth at several scales as subsurface (civil engineering), crustal, regional or global. These methods, like Full Waveform Inversion (FWI), are still in development and are mostly validated using synthetic data which are generally computed using the same wave propagation modeling engine used in the inverse problem process. In other terms, the synthetic data are computed with some assumptions (for example acoustic approximation or two-dimensional) which are the same in the inverse problem. Although, this *inverse crime* (Virigin, 2004) is particularly useful to validate an algorithm in its early development stage, it does not allow to assess the efficiency of the method for real seismic data. Moreover, because no one known precisely the Earth interior, it is difficult to evaluate the capacity of a method to recover physical parameters and structures from real seismic data which can lead sometimes to geological interpretation of numerical artefacts (Morozov, 2004). Thus, it is necessary to add a step for which imaging methods will be tested for experimental seismic measurements obtained under controlled conditions.

The best way to satisfy this need is to use Physical Small Scale Modeling Methods (noted *PSM* subsequently). *PSM* were used since several years to study the propagation of waves in various media with several stage of complexity, from acoustic wave propagation in homogeneous media to elastic wave propagation in three-dimensional heterogeneous anisotropic media (Rieber, 1936; Howes et al., 1953; Hilterman, 1970; French, 1974; Bishop et al., 1985;

Pratt, 1999; Favretto-Cristini et al., 2013; Sarkar et al., 2003; Isaac and Lawton, 1999), and allow to generate experimental seismic data under well-controlled conditions. Some methods exist to produce this kind of data for different purpose (Wong et al., 2009) and the MUSC Laboratory (Bretaud et al., 2008, 2011, 2013), *Mesure Ultrasonore Sans Contact* in French, in one of them. MUSC is designed to allow (1) wide-angle on-shore acquisitions modeling both body waves and surface waves, (2) automatic multisource-multireceiver measurements with a high-productivity, (3) high-precision source-receiver positioning and (4) high-precision recording of absolute surface displacement without coupling effects.

Our objective here is to increase the potential of the MUSC system as a reliable tool for generating experimental data which will be distributed in the scientific community. Thus we present two studies of experimental data in order to : 1) refine the comparison between numerical and experimental data by taking into account the 2D/3D effects through an alternative way and 2) identify the reproducibility of the source impact. These approaches complete the knowledge of the system and facilitate the achievement of massive multi-source and multi-receiver data simulating subsurface seismic experimental campaigns.

To achieve these objectives, we used a seismic wave modeling code based on the Spectral Element Method (Komatitsch et al., 1998; Komatitsch and Tromp, 1999; Komatitsch et al., 2005; Festa and Vilotte, 2005). This method has several advantages compared to finite differences and finite elements, such as: (1) a weak formulation which can naturally take into account the free surface, (2) an explicit scheme in time facilitating parallelization and reducing the computational cost, (3) a spatial discretization (mesh) convenient for the representation of complex environments and (4) high precision results and low numerical dispersion.

Thus, we present two coupled studies of experimental data in order to: (1) refine the comparison between numerical and experimental data by taking into account the geometrical spreading effects between two-dimensional and three-dimensional data through an alternative way, and (2) identify the reproducibility of the source impact to [...].

METHODS

Physical modeling: MUSC Bench

The MUSC bench (Bretaudau et al., 2008, 2011, 2013) is built to experimentally reproduce field seismic data with a great accuracy on small scale model 1. The bench is composed of a honeycomb tab and two arms which control the source and the receiver position with a precision of $10 \mu\text{m}$.

The receiving system of MUSC Laboratory is composed of a laser interferometer. The principle of this laser is based on a phase shift of the reflected laser signal due to the wave propagation in the material. A real-time calibration value enables a continuous conversion to a nanometric displacement. The focal diameter of the laser on the model surface is about several micrometers and allows a detection limit of 2.5 nm in the frequency range from 30 kHz to 20 MHz.

The seismic source is simulated by a piezoelectric transducer relied to a launching and synchronisation system. This system provides more energy than a laser impulse source (Bretaudau, 2010; Bretaudau et al., 2011) and allows to choose the source in terms of waveform, *i.e.*, Gauss source, Ricker source, central frequency f_0 and time delay t_0 . The source is generated by a waveform generator and is then amplified before transmitted to the small-scale-model. In the framework of seismic physical modeling, the source must be as

closed as possible to a normal point source. Thus, the piezo-electric source is coupled with an adaptater in order to reproduce the spatial energy repartition (limitating directivity) and conserving the waveform as shown in figure 3.

For the purpose of small scale modeling, the change of scale must keep the relationship between observables. For most of seismic imaging methods, the significant physical parameters are the compressional and shear waves velocities, V_P and V_S respectively, the density ρ and the quality factor Q . When scaling the model, many parameters can be modified: the distances, the time scale, the amplitudes of the signals, the visco-elastic properties, etc. Hence, the predominant factor is the wavelength $\lambda = V/f$, where V is the wave velocity and f the frequency. Thus, physical and mechanical parameters are modified to preserve the ratio $\lambda_{real} = \xi \lambda_{scale}$ where ξ is the scale ratio. It is therefore necessary to act directly on the time-frequency scales. Assuming the materials used to build the small scale model have the same mechanical properties (V_P , V_S , ρ) than the natural media, it is straightforward to obtain the scale ratios for parameters involved in seismic experiment.

For near surface experiments, the scale ratio ξ is about 1000 which means that the central frequency f_0 of the source is few kHz (generally 100 kHz but can be more or less), distances are in mm (acquisition length around 50 mm typically) and time unit is ms.

Small-scale models are generally made of metal, thermoplastic or melted epoxy resin-based materials (Bretaudau et al., 2013, 2011, 2008). These materials allow to reproduce complex geometries and have a large panel of physical and mechanical properties. These materials have the advantages to have physical properties closed to natural soil materials. The models are generally oversized to easily separate reflected waves on boundaries from the rest of the signal.

Numerical modeling: Spectral Element Method

Various numerical methods exist to resolve the equation of motion in arbitrary elastic media. The most widely used is the Finite-Differences (FD) method (Virieux, 1986; Levander, 1988; Robertsson et al., 1994; Pratt, 1990; Stekl and Pratt, 1998; Saenger and Bohlen, 2004) which estimates each derivative on a regular cartesian grid using a Taylor development (Moczo et al., 2004) of order n . FD is simple to implement but quickly shows some limitations: the cartesian grid is defined by the minimum propagated wavelenght (λ_{min}) in the full media and is unable to reproduce properly complex topography and interfaces. Moreover, Saenger et al. (2000) show that 60 points by wavelenght (λ) are needed to modelise Rayleigh wave in order $n = 2$ where only 15 points by λ are required for body waves which increases drastically the numerical cost in case of near-surface modeling experiment.

The Finite-Elements Method (FEM) is another popular method used for wave propagation modeling. FEM is based on a variationnal formulation of the equation of motion and gives a continuous approximate solution in space using polynomial basis functions defined on each node of each cell of the mesh. The natural boundary conditions of FEM is the free surface and the triangular (in 2D) or tetraedric (in 3D) unstructured meshes are well adapted to complex media and topography. However, low polynomial basis are inadequate with fine spatial discretisation and the required discretisation to obtain precise and non-dispersive solution in numerically costly.

Recently, the Spectral Element Method (SEM), used in fluid dynamics, was adapted to seismic wave propagation.

The SEM is based upon a high-order piecewise polynomial approximation of the weak formulation of the wave equation. It combines the accuracy of the pseudo-spectral method

with the flexibility of the finite-element method (Tromp et al., 2008).

In this method, the wavefield is represented in terms of high-degree Lagrange interpolants, and integrals are computed based upon GaussLobattoLegendre (gll) quadrature. This combination leading to a perfectly diagonal mass matrix leads in turn to a fully explicit time scheme which lends itself very well to numerical simulations on parallel computers. It is particularly well suited to handling complex geometries and interface matching conditions (Cristini and Komatitsch, 2012).

The typical element size that is required to generate an accurate mesh is of the order of λ , λ being the smallest wavelength of waves traveling in the model.

Models are meshed in 2D with quadrangles using the open-source software package GMSH (Geuzaine and Remacle, 2009).

RESULTS

From point-source to line-source acquisition

In the framework of wave propagation modeling and waveform inversion, most of available algorithms are limited to the two-dimensional approximation especially for computational cost causes. Thus, line-source seismograms are required as observed data to be compared to synthetic seismograms or for inversion processes.

However, MUSC is designed to produce three-dimensional experimental seismograms from a piezo-electric source selected to be as closed as possible to a point source. Generally, the correction of the geometrical spreading is done by convolving each trace by $\sqrt{t^{-1}}$, where t is the traveltime, with or without offset conditioning. The correct phase can then be obtained

using a source wavelet estimation method (Bretaud et al., 2011).

Recently, Forbriger et al. (2014) and Schafer et al. (2014) have developed, and successfully applied to synthetic seismogram, an hybrid method to convert the three-dimensional geometrical spreading in two-dimensional spreading using both convolution tapering and offset dependent scaling of the waveform. However, these pre-processing methods are not perfect and can not be easily automated and the results are strongly conditioned by user's experience and attempts.

Here, we take advantage of the experimental framework to explore an alternative approach specific to MUSC. Contrary to field experiments, it is possible to generate a pseudo-line-source finely sampled by multiple point-sources, perpendicular to the acquisition line.

Each point-source must be enough close each other so the resulting source being a line-source in the sense of Huygens principle. To do that, we consider that the length of the line must be equal, at least, $L \geq 4\lambda_{max}$ and the sampling interval $ds \leq 10/\lambda_{min}$. Given the material's properties, we choose $L = 240 \text{ mm}$ and $ds = 0.5 \text{ mm}$ which leads to 481 point-source locations. The line of point-source is located at ?? mm distance. Four receiver positions have been selected: 90, 95, 100 and 105 mm offset from the source. The source wavelet is a Ricker with a central frequency $f_0 = 100 \text{ kHz}$. Each receiver is perpendicular to and centered on the line-source. For each receiver position, the complete signal is stack along source position to obtain an equivalent two-dimensional line-source response.

To evaluate the efficiency of the method, experimental line-source responses will be compared to point-source and equivalent line-source responses using the cross-correlation coefficient (**cc**) and the root mean square (**rms**) ratio. These values are presented in table 1. **cc_{init}** and **rms_{init}** correspond to direct evaluation whereas **cc_{final}** corresponds to the

best **cc** obtained and **rms_{final}** is the corresponding **rms**.

Figures 6(a,b,c,d) show the comparison between experimental traces obtained using a point-source and a line-source for source-receiver offsets 90, 95, 100 and 105 mm respectively. It is straightforward that these waveforms are not similar in terms of both phases (**cc**<0.2) and amplitude (**rms**>1.2). Even after dephasing point-source response to the line-response in term of phase (**cc**>0.6), amplitudes do not match (**rms**>0.6). These results confirm that using raw point-source responses in a two-dimensional inversion process or imaging method can be critical in terms of convergence and validity of the results since these methods are built over phase and/or amplitude similarity.

Figures 6(e,f,g,h) show the comparison between experimental traces using a line-source and a point-source after geometrical spreading corrections (equivalent line-source response) for the same previous source-receiver offsets. The cross-correlation coefficient **cc** for these waveforms are greater than 0.69 but with **rms** greater than 0.66 and between 0.48 and 0.54 after phase fitting (**cc**>0.85). These results denote that the experimental line-source response is correct in terms of phase compared to an equivalent line-source response. However, **rms** are still great even if they are smaller than previously. This can be explained by small differences in terms of waveforms and phases which are critical in the final **rms** results. Moreover, the *hybrid* method to obtain the equivalent line-source response from a point-source response needs accurate parametrisation to obtain the best result which is not necessarily in a good agreement with the attempt true line-source response.

These results show that the line-source emulation on the MUSC laboratory is efficient and can produce data suitable for imaging methods such as 2D FWI.

Experimental source reproducibility

To assess the ability of MUSC to provide reproducible data, *i.e.* to evaluate the reproducibility of the source impact, several physical modeling were performed on a homogeneous epoxy-resin block for which the seismic waves velocities and the intrinsic attenuation are known : $V_P = 2300 \text{ m.s}^{-1}$, $V_S = 1030 \text{ m.s}^{-1}$, $\rho = 1300 \text{ kg.m}^{-3}$ and $Q = 30$.

Six realizations have been acquired on this model with a similar geometry setup, *i.e.* 121 receivers positions with an increment equal to 1 mm and a minimum offset of 10 mm. The numerical wavelet sent to the piezoelectric transducer source is a Ricker signal with a central frequency of 100 kHz. However, the source waveform is modified by the physical coupling effect of the transducer.

First, source wavelet were estimated for each experiment (Figure 7(a)) using a linear source wavelet estimation method based on a stabilized deconvolution (Pratt, 1999). The effective sources show different oscillations after the main pulse, due to internal echoes in the transducer. These secondary oscillations have a very similar shape from an experiment to another, as well as the global signal shape even if some small differences of amplitudes appear for the main pulse. Figure 7(b,c,d,e,f,g) show numerically propagated signals after convolution with estimated source wavelets for the offset of 60 mm. The corrected numerical seismograms are in good agreement with the experimental seismograms. The value of the correlation coefficient (> 0.98 , also presented in the figure) confirms the great efficiency of the wavelet source assessment process.

In a second step, a unique source wavelet is estimated by taking into account the 6 experiments together (figure 9(a)). The resulting source parameters were applied to the synthetic signals (figure 9(b,c,d,e,f,g)) for the same receiver position as previously. As in the previous

case, the corrected seismograms are in good agreement with the experimental seismograms (correlation coefficients > 0.96).

These last results, based on an average estimated source wavelet show that the effective impulse source emitted by the transducer in the MUSC measurement bench is stable enough to ensure a robust reproducibility of the source. Therefore, concerning the key issue of the source knowledge, experimental data acquired in the MUSC laboratory can be efficiently processed by imaging methods like Full Waveform Inversion (FWI) with only one estimation step for all the multi-source and multi-receivers data.

CONCLUSIONS

These two studies allow to refine the capacity of the physical modeling designed for seismic experiments simulation by 1) completing the validation of the measurement through comparison of numerical and experimental data generated by a realistic 2D source line and 2) assessing the reproducibility of the effective source emitted in a model. These improvements allow to provide and distribute experimental reduced scale data to the scientific community as benchmark datasets.

PLOTS

Equations

Figures

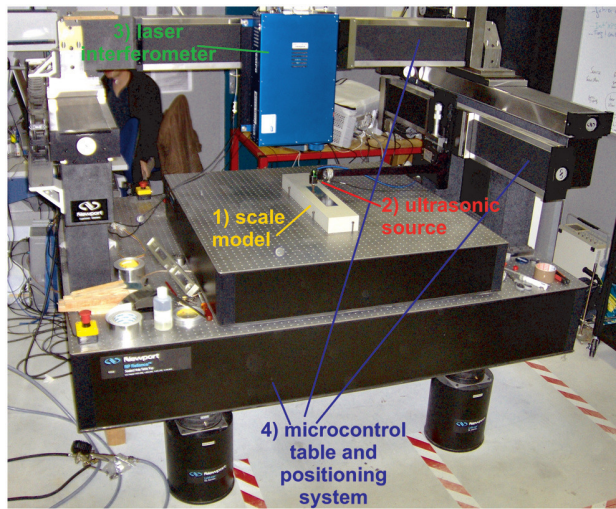


Figure 1: Photograph of the MUSC ultrasonic laboratory (from Breteau et al. (2013)) with its four components: (1) a small-scale model of the underground, (2) an optical table with two automated arms moving above the model, (3) a laser interferometer recording ultrasonic wave propagation at the model surface, and (4) a piezoelectric ultrasonic source generating ultrasonic waves in the model.

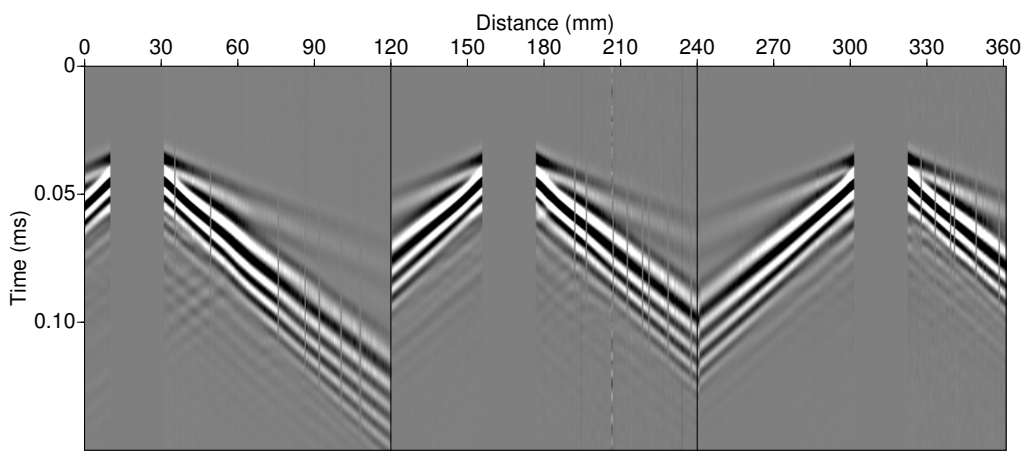


Figure 2: Example of multi-source multi-receiver record on the MUSC bench for a two-layer model (biault).

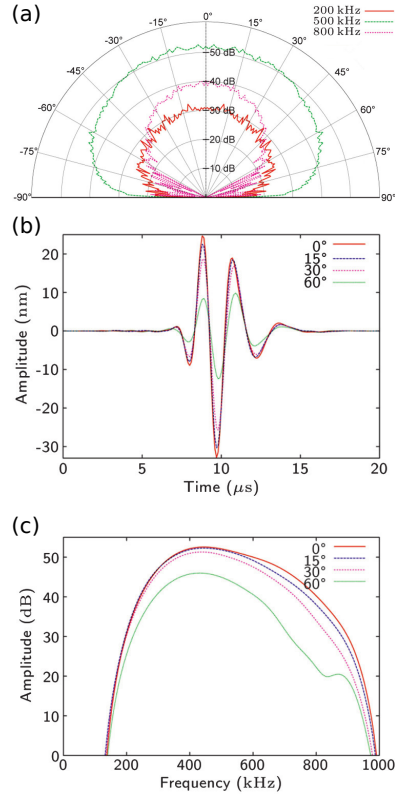


Figure 3: Validation of the piezo-electric source coupled with an adaptater (Bretaudéau et al., 2011). (a) Directivity diagrams (dB) for the high-frequency source Panametrics® with conical polyurethane adapter: three frequencies normal particle displacement. (b) Temporal signals and (c) amplitude spectrums for the high-frequency source Panametrics® with a conical polyurethane adapter in transmission through a PVC cylinder for various angles of incidence: 0, 15, 30, and 60 degrees normal particle displacement.

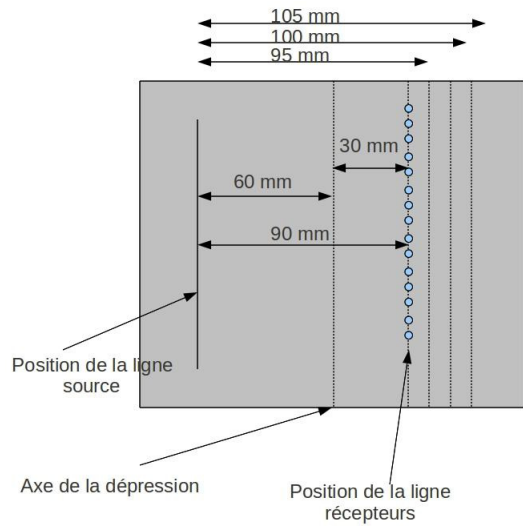


Figure 4: .

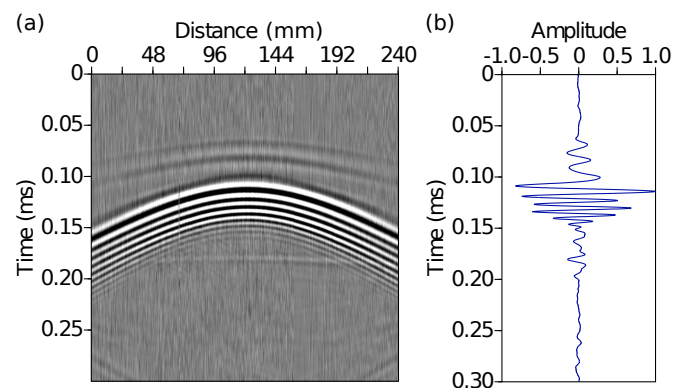


Figure 5: .

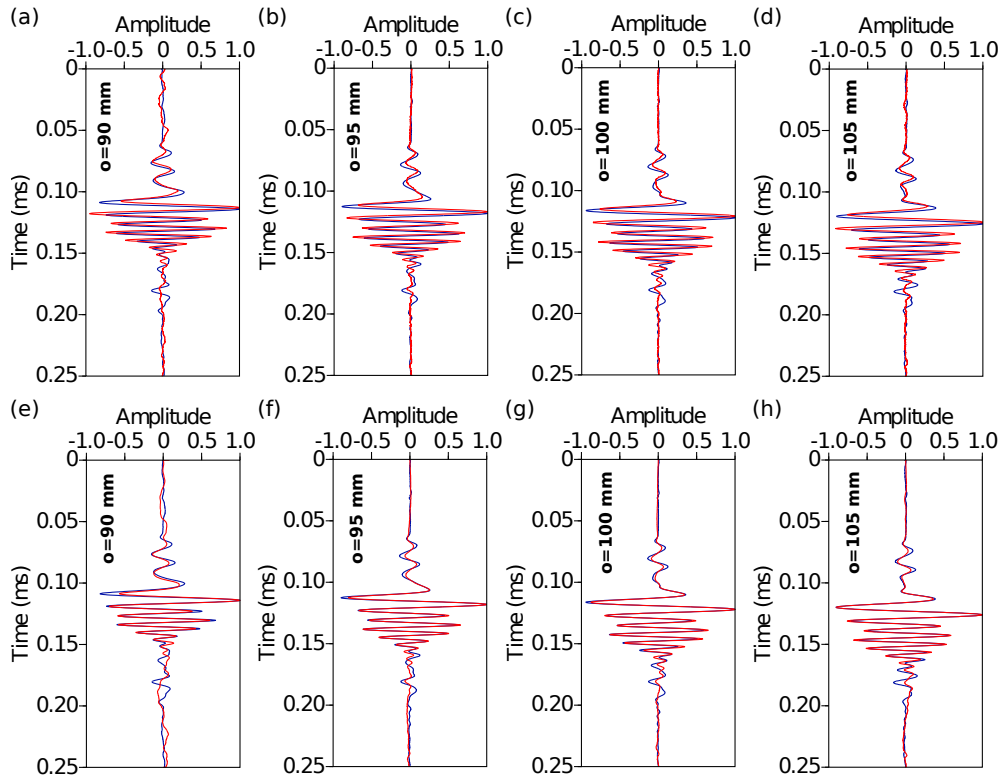


Figure 6: (a,b,c,d) Comparison between an experimental seismogram for a point-source (red), an experimental seismogram for a line-source (blue) for 90, 95, 100 and 105 mm offset respectively. (e,f,g,h) Comparison between an experimental seismogram for a line-source (blue), and for a point-source corrected from geometrical spreading (green) for 90, 95, 100 and 105 mm offset respectively r gives the correlation factor between numerical simulation from the estimated effective source and experimental traces.

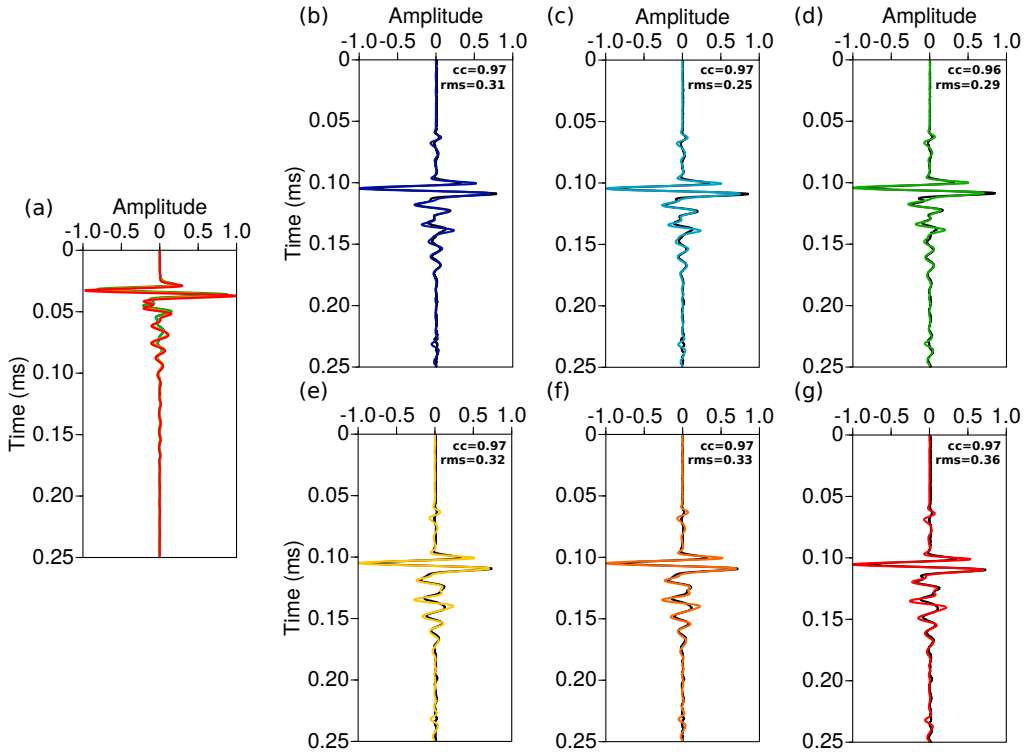


Figure 7: (a) Comparison between six estimated source wavelets (*ESW*) calculated for each experiment. (b,c,d,e,f,g) Comparison between experimental traces (black) and numerically simulated traces corrected with the corresponding estimated effective source (colored). r gives the correlation factor between numerical simulation from the estimated effective source and experimental traces.

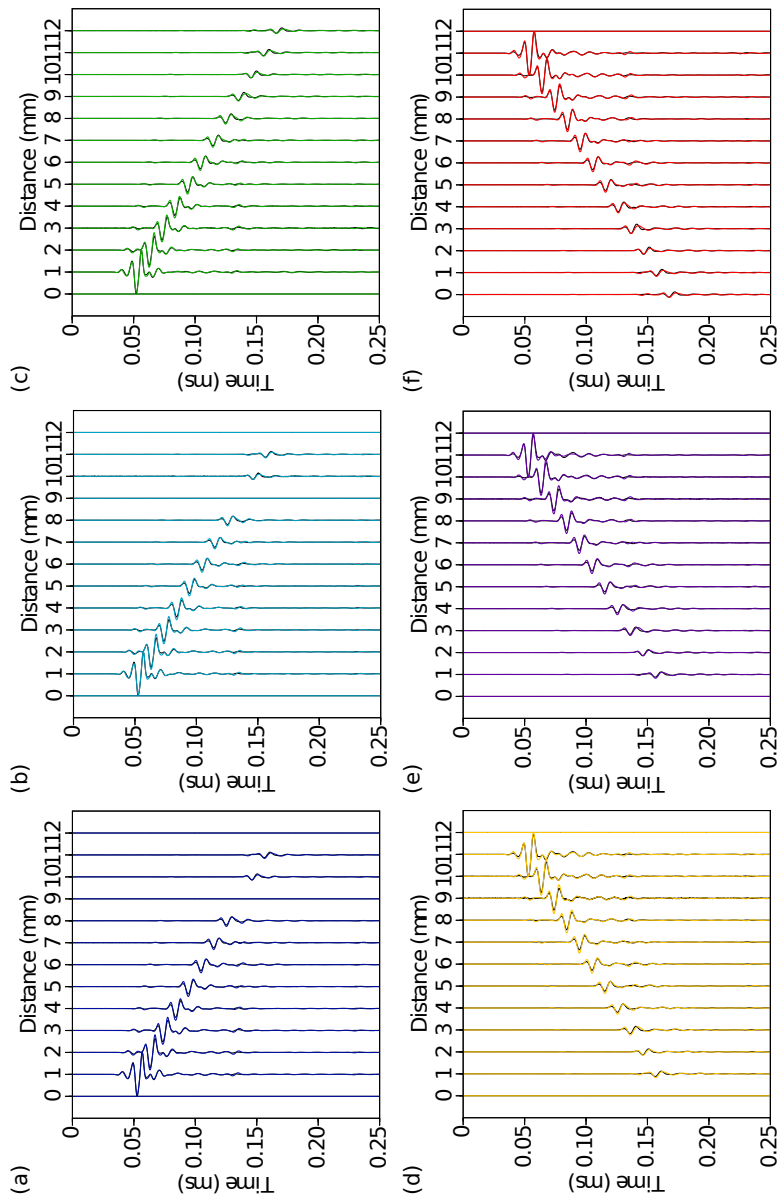


Figure 8: .

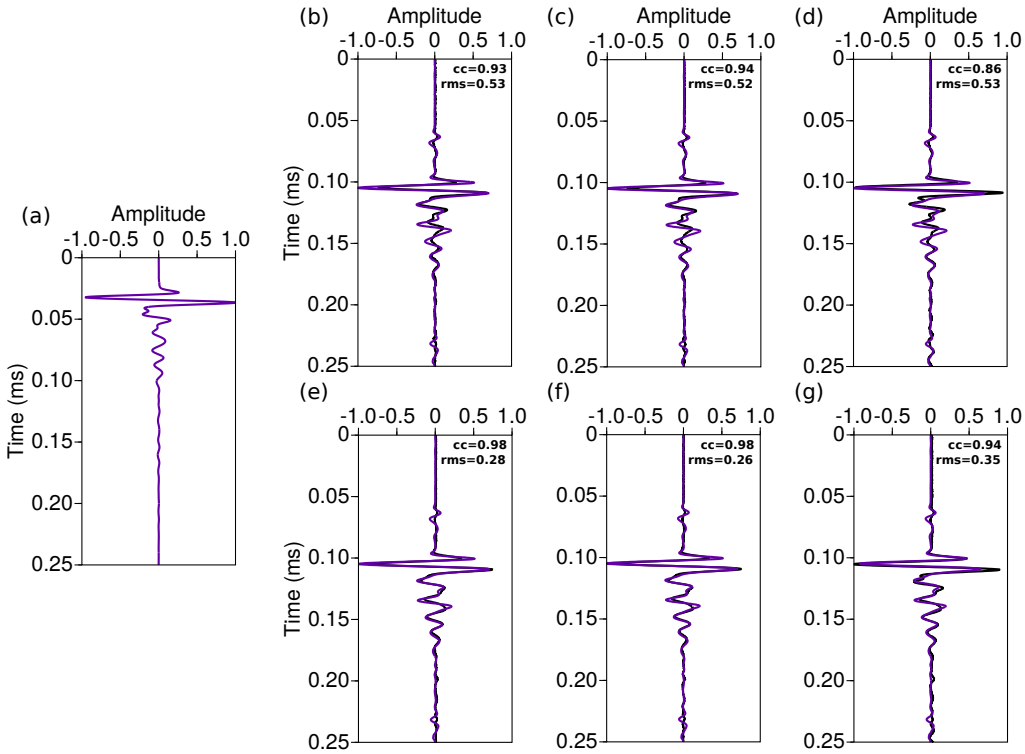


Figure 9: (a) Estimated source wavelet (*ESW*) calculated for all experiments. (b,c,d,e,f,g,h)

Comparison between experimental traces (black) and numerically simulated traces corrected with the corresponding estimated effective source (colored). r gives the correlation factor between numerical simulation from the estimated effective source and experimental traces.

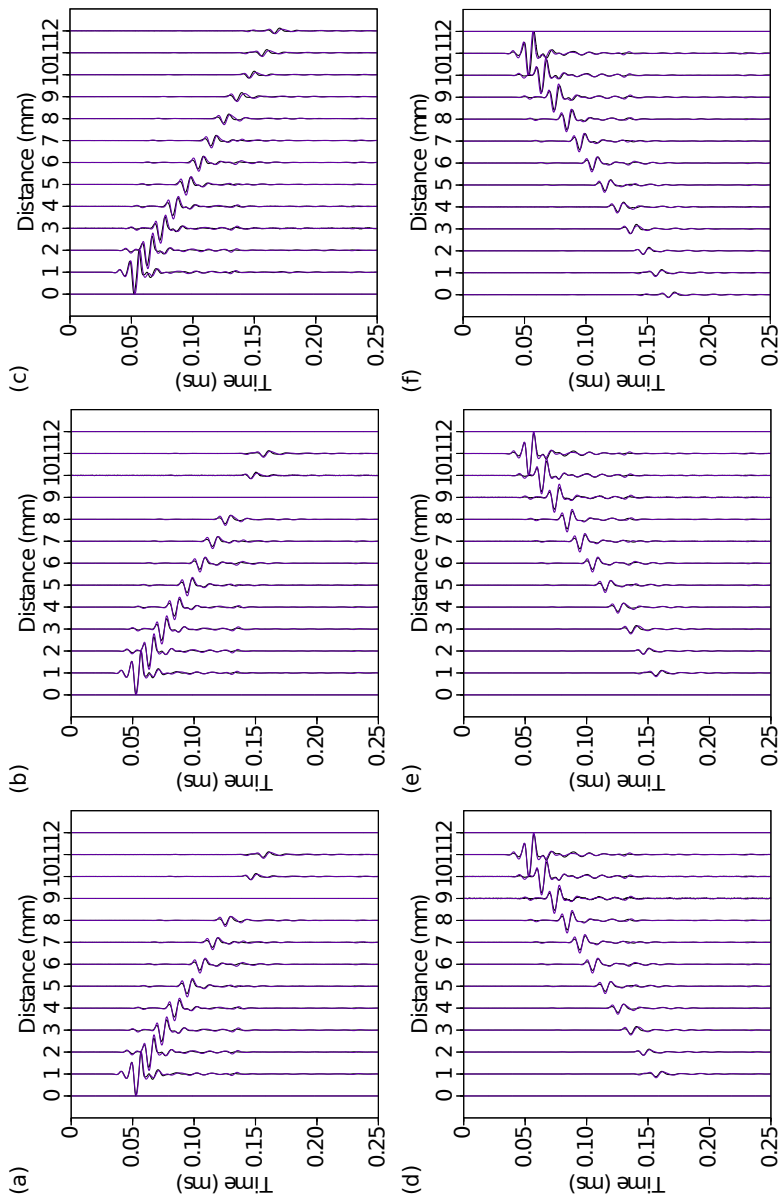


Figure 10: .

Tables

	90 mm	95 mm	100 mm	105 mm
$cc1_{init}$	0.702	0.725	0.728	0.728
$rms1_{init}$	0.794	0.760	0.762	0.774
$cc1_{final}$	0.940	0.953	0.951	0.949
$rms1_{final}$	0.358	0.317	0.325	0.343
$cc2_{init}$	0.954	0.987	0.988	0.988
$rms2_{init}$	0.304	0.162	0.155	0.154
$cc2_{final}$	—	—	—	—
$rms2_{final}$	—	—	—	—

Table 1: .

ACKNOWLEDGMENTS

REFERENCES

- Ammon, C. J., 1991, The isolation of receiver effects from teleseismic p waveform: Bulletin of Seismological Society of America, **81**, 2504–2510.
- Bishop, T., K. Bube, R. Cutler, R. Langan, P. Love, J. Resnick, R. Shuey, and D. Spindler, 1985, Tomographic determination of velocity and depth in laterally varying media: Geophysics, **50**, 903–923.
- Bretaudeau, F., 2010, Modélisation physique à échelle réduite pour l'adaptation de l'inversion des formes d'ondes sismiques au génie civil et à la subsurface: PhD thesis, Université de Nantes.
- Bretaudeau, F., R. Brossier, D. Leparoux, O. Abraham, and J. Virieux, 2013, 2d elastic full-waveform imaging of the near-surface: application to synthetic and physical modelling data sets: Near Surface Geophysics.
- Bretaudeau, F., D. Leparoux, and O. Abraham, 2008, Small scale adaptation of the seismic full waveform inversion method - application to civil engineering applications.: The Journal of the Acoustical Society of America, **123**.
- Bretaudeau, F., D. Leparoux, O. Durand, and O. Abraham, 2011, Small-scale modeling of onshore seismic experiment: A tool to validate numerical modeling and seismic imaging methods: Geophysics, **76(5)**, T101–T112.
- Cristini, P., and D. Komatitsch, 2012, Some illustrative examples of the use of the spectral-element method in ocean acoustics.: Journal of the Acoustical Society of America.
- Favretto-Cristini, N., A. Tantsereva, P. Cristini, B. Ursin, D. Komatitsch, and A. Aizenberg, 2013, Numerical modeling of zero-offset laboratory data in a strong topographic environment: results for a spectral-element method and a discretized kirchhoff integral method: Earthquake Science.

- Festa, G., and J. Vilotte, 2005, The Newmark as velocity-stress time-staggering: an efficient PML implementation for spectral element simulation of elastodynamics: *Geophysical Journal International*, **161**, 798–812.
- Forbriger, T., L. Gross, and M. Schafer, 2014, Line-source simulation for shallow-seismic data. part 1: theoretical background: *Geophysical Journal International*, **198**, 1387–1404.
- French, W. S., 1974, Two-dimensional and three-dimensional migration of model-experiment reflection profiles: *Geophysics*, **39(3)**, 265–277.
- Geuzaine, C., and J. Remacle, 2009, Gmsh: a three-dimensional finite element mesh generator with built-in pre- and post-processing facilities.: *International Journal for Numerical Methods in Engineering*, **79**, 1309–1331.
- Hilterman, F., 1970, Three-dimensional seismic modeling: *Geophysics*, **35**, 1020–1037.
- Howes, E., L. Tejada-Flores, and L. Randolph, 1953, Seismic model study: *Journal of the Acoustical Society of America*, **25**, 915–921.
- Isaac, J. H., and D. C. Lawton, 1999, Image mispositioning due to dipping media: A physical seismic modeling study: *Geophysics*, **64**, 1230–1238.
- Jones, I. F., 2013, A practical review of migration issues and solutions: Presented at the Subsurface Challenges in West Africa-First EAGE West Africa Workshop.
- Komatitsch, D., and J. Tromp, 1999, Introduction to the spectral-element method for three-dimensional seismic wave propagation: *Geophysical Journal International*, **139**, 806–822.
- Komatitsch, D., S. Tsuboi, and J. Tromp, 2005, The spectral-element method in seismology.
- Komatitsch, D., J. P. Vilotte, R. Vai, J. M. Castillo-Covarrubias, and F. J. Sánchez-Sesma, 1998, The Spectral Element Method for Elastic Wave Equation: Application to 2-D and 3-D Seismic Problems: *International Journal for Numerical Methods in Engineering*, **45**, 1139–1164.

- Levander, A., 1988, Fourth-order finite-difference p-sv seismograms: *Geophysics*, **53**, 1425–1436.
- Moczo, P., J. Kristek, and L. Halada, 2004, The finite-differences method for seismologists: An introduction: Comenius University, Bratislava.
- Montelli, R., G. Nolet, F. A. Dahlen, G. Masters, E. R. Engdahl, and S. H. Hung, 2004, Finite-frequency tomography reveals a variety of plumes in the mantle: *Science*, **303**, 338–343.
- Morozov, I., 2004, Crustal scattering and some artefacts in receiver function images: *Bulletin of the Seismological Society of America*, **94**, 1492–1499.
- Pratt, R. G., 1990, Frequency domain elastic wave modeling by finite differences: A tool for cross-hole seismic imaging.: *Geophysics*, **55**, 626–632.
- , 1999, Seismic waveform inversion in the frequency domain, Part 1: Theory and verification in a physical scale model: *Geophysics*, **64**, 888–901.
- Rieber, F., 1936, Visual presentation of elastic wave patterns under various structural conditions: *Geophysics*, **1**, 196–218.
- Robertsson, J., J. Blanch, and W. Symes, 1994, Viscoelastic finite-difference modeling.: *Geophysics*, **59**, 1444–1456.
- Saenger, E. H., and T. Bohlen, 2004, Finite-difference modeling of viscoelastic and anisotropic wave propagation using the rotated staggered grid: *Geophysics*, **69**, 583–591.
- Saenger, E. H., N. Gold, and A. Shapiro, 2000, Modeling the propagation of elastic waves using a modified finite-difference grid: *Wave Motion*, **31**, 77–92.
- Sarkar, D., A. Bakulin, and R. L. Kranz, 2003, Anisotropic inversion of seismic data for stressed media: Theory and a physical modeling study on berea sandstone: *Geophysics*, **68**, 1–15.

- Schafer, M., L. Gross, T. Forbriger, and T. Bohlen, 2014, Line-source simulation for shallow-seismic data. part2: full-waveform inversion – a synthetic 2-d case study: *Geophysical Journal International*, **198**, 1405–1418.
- Stekl, I., and R. G. Pratt, 1998, Accurate visco-elastic modeling by frequency-domain finite differences, using rotated operators.: *Geophysics*, **63**, 1779–1794.
- Tromp, J., D. Komatitsch, and Q. Liu, 2008, Spectral-element and adjoint methods in seismology.: *Commun Comput Phys*.
- Virieux, J., 1986, P-sv wave propagation in heterogeneous media: velocity-stress finite-difference method: *Geophysics*, **51**, 889–901.
- Virieux, J., and S. Operto, 2009, An overview of full-waveform inversion in exploration geophysics: *Geophysics*, **74**, WCC1WCC26.
- Wirgin, A., 2004, The inverse crime: ArXiv Mathematical Physics e-prints. (Provided by the SAO/NASA Astrophysics Data System).
- Wong, J., K. W. Hall, E. V. Gallant, R. Maier, M. Bertram, and D. C. Lawton, 2009, Seismic physical modeling at university of calgary: CSEG recorder, **34**.